

UC San Diego

UC San Diego Previously Published Works

Title

Comparison of synthesized and acquired high b-value diffusion-weighted MRI for detection of prostate cancer

Permalink

<https://escholarship.org/uc/item/4vk4v9nb>

Journal

Cancer Imaging, 24(1)

ISSN

1740-5025

Authors

Kallis, Karoline

Conlin, Christopher C

Zhong, Allison Y

et al.

Publication Date

2024

DOI

10.1186/s40644-024-00723-6

Copyright Information

This work is made available under the terms of a Creative Commons Attribution License, available at <https://creativecommons.org/licenses/by/4.0/>


Peer reviewed

RESEARCH ARTICLE

Open Access



Comparison of synthesized and acquired high b -value diffusion-weighted MRI for detection of prostate cancer

Karoline Kallis², Christopher C. Conlin¹, Allison Y. Zhong², Troy S. Hussain², Aritrick Chatterjee^{6,7}, Gregory S. Karczmar^{6,7}, Rebecca Rakow-Penner¹, Anders M. Dale^{1,3,4} and Tyler M. Seibert^{1,2,5*} 

Abstract

Background High b -value diffusion-weighted images (DWI) are used for detection of clinically significant prostate cancer (csPCa). This study qualitatively and quantitatively compares synthesized DWI (sDWI) to acquired (aDWI) for detection of csPCa.

Methods One hundred fifty-one consecutive patients who underwent prostate MRI and biopsy were included in the study. Axial DWI with $b=0, 500, 1000,$ and 2000 s/mm² using a 3T clinical scanner using a 32-channel phased-array body coil were acquired. We retrospectively synthesized DWI for $b=2000$ s/mm² via extrapolation based on mono-exponential decay, using $b=0$ and $b=500$ s/mm² (sDWI₅₀₀) and $b=0, b=500$ s/mm², and $b=1000$ s/mm² (sDWI₁₀₀₀). Differences in signal intensity between sDWI and aDWI were evaluated within different regions of interest (prostate alone, prostate plus 5 mm, 30 mm and 70 mm margin and full field of view). The maximum DWI value within each ROI was evaluated for prediction of csPCa. Classification accuracy was compared to Restriction Spectrum Imaging restriction score (RSIs), a previously validated biomarker based on multi-exponential DWI. Discrimination of csPCa was evaluated via area under the receiver operating characteristic curve (AUC).

Results Within the prostate, mean \pm standard deviation of percent mean differences between sDWI and aDWI signal were $-46 \pm 35\%$ for sDWI₁₀₀₀ and $-67 \pm 24\%$ for sDWI₅₀₀. AUC for aDWI, sDWI₅₀₀, sDWI₁₀₀₀, and RSIs within the prostate 0.62[95% confidence interval: 0.53, 0.71], 0.63[0.54, 0.72], 0.65[0.56, 0.73] and 0.78[0.71, 0.86], respectively.

Conclusion sDWI is qualitatively comparable to aDWI within the prostate. However, hyperintense artifacts are introduced with sDWI in the surrounding pelvic tissue that interfere with quantitative cancer detection and might mask metastases. In the prostate, RSIs yields superior quantitative csPCa detection than sDWI or aDWI.

Keywords Diffusion-weighted imaging, Prostate cancer, Synthetic high b -values, Restricted Spectrum Imaging

*Correspondence:

Tyler M. Seibert

tseibert@health.ucsd.edu

Full list of author information is available at the end of the article



© The Author(s) 2024. **Open Access** This article is licensed under a Creative Commons Attribution 4.0 International License, which permits use, sharing, adaptation, distribution and reproduction in any medium or format, as long as you give appropriate credit to the original author(s) and the source, provide a link to the Creative Commons licence, and indicate if changes were made. The images or other third party material in this article are included in the article's Creative Commons licence, unless indicated otherwise in a credit line to the material. If material is not included in the article's Creative Commons licence and your intended use is not permitted by statutory regulation or exceeds the permitted use, you will need to obtain permission directly from the copyright holder. To view a copy of this licence, visit <http://creativecommons.org/licenses/by/4.0/>. The Creative Commons Public Domain Dedication waiver (<http://creativecommons.org/publicdomain/zero/1.0/>) applies to the data made available in this article, unless otherwise stated in a credit line to the data.

Background

Diffusion-weighted imaging (DWI) is a critical component of multiparametric MRI for the detection and characterization of clinically significant prostate cancer (csPCa) [1]. The degree of diffusion-weighting in DWI is indicated by the b -value, with higher b -values corresponding to images with less signal where water in tissues diffuses more rapidly [2]. High b -values are used for their greater tumor conspicuity and detection of even small lesions [3]. The Prostate Imaging – Reporting and Data System (PI-RADS v2.1) recommends the acquisition of high b -values (1400–2000s/mm²) for lesion detection, without precisely defining an optimal value for csPCa [4]. While clinically valuable, high b -values require more scan time and suffer from low signal-to-noise ratio (SNR) and increased susceptibility to artifacts due to microscopic motion or small fluctuations in local magnetic field. One common solution, permitted by PI-RADS, is to synthesize high b -value images by extrapolating signal from acquired low b -value images using a mono-exponential model [1, 5]. However, mono-exponential models do not adequately represent restricted diffusion in complex tissues [6, 7], possibly calling into question the accuracy of synthesized images.

More advanced DWI models have been developed to better account for tissue microstructure, including intra-voxel incoherent motion imaging [8, 9], diffusion kurtosis imaging [10, 11], Vascular, Extracellular, and Restricted Diffusion for Cytometry in Tumor (VERDICT) [12–14], hybrid multidimensional MRI (HM-MRI) [15–18], and Restriction Spectrum imaging (RSI) [12, 19]. In RSI, the diffusion signal is modeled as a weighted sum of different compartments representing different tissue types [19, 20]. The RSI restriction score (RSIRs) is based on the model coefficient for the most restricted diffusion compartment and has been shown to be a useful biomarker for the detection of csPCa [20–22].

Studies have yielded contradicting results on whether synthesized b -values are clinically interchangeable with acquired DWI (aDWI) images. Liu et al. [23] compared various models, including the standard mono-exponential, for the detection of csPCa and concluded that non-linear fitting with various b -values is superior to simpler models. In contrast, other studies reported better image quality for synthetic DWI (sDWI) with a similar tumor detection rate in comparison to acquired DWI [5, 24–27].

In this study, we qualitatively and quantitatively analyzed the differences between acquired and synthesized high b -value images for detection of csPCa. Further, we evaluated acquired and synthesized high b -value DWI for detection of csPCa at the patient level. For comparison, we also evaluated RSIRs, a quantitative biomarker based

on multi-compartment DWI that is known to perform well for patient-level csPCa detection.

Methods

Patient cohort

This retrospective study was approved by the institutional review board at UC San Diego (IRB 805394). The research was performed in accordance with the Declaration of Helsinki, and all relevant regulations. A waiver of consent was approved by the institutional review board for this study as there was minimal risk of harm to patients. The retrospective dataset was described previously [22]. Briefly, 440 consecutive men who underwent prostate MRI examination with a multi- b -value diffusion acquisition (compatible with Restriction Spectrum Imaging, RSI) between November 2017 and December 2020 were considered for inclusion. Patients were excluded if they had undergone prior treatment for prostate cancer or if there was no available biopsy result performed within 180 days of MRI acquisition. In total 151 patients were included in the study. Patient characteristics are summarized in Table 1.

Table 1 Patient Characteristics range Q_1 – Q_3 Range between lower first quartile to upper third quartile, csPCa Clinically significant prostate cancer, MRI Magnet resonance imaging, PSA Prostate-specific antigen

Parameter	Specification	Value
Number of patients	Total	151
Age [a]	Median (range Q_1 – Q_3)	66 (59–72)
Time from MRI to biopsy [d]	Median (range Q_1 – Q_3)	16 (1–35)
PSA at time of MRI [ng/ml]	Median (range Q_1 – Q_3)	7.3 (5.3–10.4)
Prostate volume [ml]	Median (range Q_1 – Q_3)	45 (34–61)
PSA density [ng/ml ²]	Median (range Q_1 – Q_3)	0.16 (0.11–0.25)
Best available pathology	Systematic	7
	Targeted	17
	Systematic and Targeted	85
	Prostatectomy	42
PI-RADS Score (csPCa)	I	0
	II	5 (3)
	III	27 (4)
	IV	55 (25)
	V	64 (54)
Gleason Grade Group	Benign	25
	1	40
	2	38
	3	20
	4	16
Clinical Tumor stage	5	12
	Negative Biopsy	25
	T1c	94
	T2a	13
	T2b	11
T2c	8	

MRI examinations were interpreted per routine clinical practice by ten board-certified (median of four years of experience) and subspecialty fellowship-trained radiologists. For all patients, suspicious lesions were contoured per PI-RADS v2.1 using MIM software (MIM Software, Inc; Cleveland, OH). For the present study, whole-gland prostate segmentation was performed using OnQ Prostate software (Cortechs Labs, San Diego, CA, USA). Clinically significant prostate cancer (csPCa) was defined as grade group ≥ 2 . In patients who underwent prostatectomy, grade group was determined per final pathology report. Biopsy (typically systematic and targeted) and prostatectomy were performed according to clinical routine, and both were examined by board-certified pathologists. 86 of the 151 patients were found to have csPCa, while 65 had only benign tissue or grade group 1 cancer (further details in Table 1).

MRI acquisition

All MRI acquisitions were performed on a 3T clinical GE scanner (Discovery MR750, GE Healthcare, Waukesha, WI, USA) using a 32-channel phased-array body coil surrounding the pelvis. Acquisition parameters are summarized in Table 2. A single axial DWI volume was acquired for each patient. T_2 -weighted reference images were acquired for all patients with field of view (FOV) identical to the DWI volume. RSI calculations were performed as described in prior studies [20–22].

Post-processing of the image data was performed using in-house software in MATLAB (version R2017a, MathWorks, Natick, MA, USA). DWI images were corrected for B_0 inhomogeneity distortions, gradient non-linearity, and eddy currents [28–30]. Multiple acquired DWI samples at specific b -values were averaged together and normalized by median signal intensity of urine in the bladder at $b = 0$ s/mm².

Table 2 Acquisition parameters for clinical multi-parametric MRI; DWI = Diffusion-weighted imaging, T2W = T_2 weighted MRI

Series	DWI	T2W
FOV [mm*mm]	240*120	320*320
Matrix (resampled dimensions)	96*48 (128*64)	320*320 (512*512)
Number of Slices	16	32
Slice thickness [mm]	6	3
TR [ms]	4500	6080
TE [ms]	68	102
b -values [s/mm ²] (number of samples)	0 (2), 500 (6), 1000 (6), 2000 (12)	N/A

Synthetic b -value computation

Synthetic high b -value DWI (sDWI) was calculated using the conventional, mono-exponential formula (see below) and using b -values up to 500 s/mm² (sDWI₅₀₀) or b -values up to 1000 s/mm² (sDWI₁₀₀₀).

$$S(b) = S_0 e^{-b ADC}$$

$S(b)$ is DWI signal for a given b -value, b . S_0 is the signal with no diffusion weighting. ADC is the apparent diffusion coefficient. sDWI was calculated for $b = 2000$ s/mm² to match the acquired high b -value DWI (aDWI). To explore the application of sDWI and aDWI for detection of significant cancer lesions outside of the prostate, sDWI and RSIs were additionally calculated for one representative patient with csPCa and bone metastasis.

Data analysis

All data analysis was performed using in-house MATLAB scripts (version R2021a, MathWorks, Natick, MA, USA). Quantitative differences between sDWI and aDWI were estimated by a voxel-wise comparison of the images. Relative deviations were calculated for three different regions of interest (ROIs): prostate, prostate plus a margin of 5 mm, and the whole field of view (FOV) using the following formula:

$$\Delta S = \frac{1}{N} \sum_{i=0}^N \frac{S_s - S_a}{S_a}$$

where S_s is the synthetic signal intensity, S_a the acquired signal and N the number of voxels in the considered images. Mean and standard deviation of ΔS over all patients are reported. A negative value indicates that the acquired signal intensity is higher than the synthesized signal intensity. Further, violin plots were generated for the 50th, 95th, and 98th percentile of signal intensity within several ROIs: prostate; prostate plus margin (5 mm, 30 mm, or 70 mm); and the whole FOV. For the whole FOV, values higher than 3000 signal intensity units (SIU) were capped and set to 3000 SIU. Violin plots present the median value in combination with the kernel density distribution [31].

Lesion conspicuity was evaluated using the contrast-to-noise ratio (CNR) between lesion and surrounding prostate tissue. CNR is defined as the following:

$$CNR = \frac{(\mu_{lesion} - \mu_{prostate})}{\sqrt{\sigma_{lesion}^2 + \sigma_{prostate}^2}}$$

where μ is the mean signal of the ROI under consideration and σ the standard deviation. CNR was evaluated for all patients and patients diagnosed with csPCa. A higher CNR indicates a better tumor conspicuity [32].

Significant differences between CNRs of different images and patient cohorts were tested using two sample t-test with a confidence level of 0.01.

Prediction of whether csPCa was found on biopsy was also evaluated for aDWI, sDWI, and RSIs. RSIs is a quantitative cancer biomarker based on a multi-exponential DWI model (four compartments) and has been previously shown to be more accurate than conventional DWI [20–22]. Computation of RSIs for this dataset was performed previously and is described in detail in previous publications [20–22]. Briefly, the coefficient for the slowest diffusion compartment (corresponding to intracellular restricted diffusion) was normalized by the median signal within the prostate on $b=0$ s/mm² images. The maximum aDWI, sDWI, or RSIs value within each considered ROI was used as the predictor variable [22]. This is analogous to the maximum standard uptake value (SUV) in quantitative Positron Emission Tomography (PET) imaging. Receiver-operating characteristic (ROC) curves were calculated, and the area under the curve (AUC) reported for aDWI, sDWI, and RSIs. The false positive rate at 90% sensitivity (FPR90) was also reported for each metric to illustrate performance at one threshold [21]. AUC and FPR90 were compared using bootstrap ($N=10,000$) 95% confidence intervals and p -values.

Results

Figure 1 shows the difference between acquired and synthesized b -values for a representative patient using the mean signal intensity within the prostate. Within the prostate, mean \pm standard deviation of percent differences between sDWI and aDWI were $-46 \pm 35\%$ for sDWI₁₀₀₀ and $-67 \pm 24\%$ for sDWI₅₀₀. A negative error indicates sDWI had lower intensity values than aDWI. Figure 2 shows aDWI, sDWI and RSIs for three representative patients with the same window and level.

Comparing sDWI₁₀₀₀ to sDWI₅₀₀, a difference of $-41 \pm 4\%$ was estimated (see Table 3). sDWI₅₀₀ had overall larger errors than sDWI₁₀₀₀. Signal intensity of sDWI was lower than aDWI in the prostate and in the prostate plus 5 mm margin considering all voxels, as indicated by a negative median difference, see Table 3. Further, a lower median value considering only the 50th, 95th and 98th percentiles was also observed. The 50th percentile of aDWI is higher than sDWI for all considered ROIs. For the 95th and 98th percentiles, however, sDWI is larger for margins of ≥ 30 mm beyond the prostate. The standard deviation of sDWI is larger than the standard deviation of aDWI for all considered percentiles in all ROIs. A comparison of the 50th, 95th and 98th percentiles for five ROIs with varying margins around the prostate is shown in Fig. 3.

Mean and standard deviation of CNR over all patients was 0.95 ± 0.87 , 0.84 ± 0.80 , 0.65 ± 0.66 and 0.97 ± 0.79

for aDWI, sDWI₁₀₀₀, sDWI₅₀₀ and RSIs, respectively. A lower CNR indicates a lower tumor conspicuity. CNR considering only patients with csPCa changed to 1.00 ± 0.84 , 0.86 ± 0.78 , 0.65 ± 0.65 and 0.99 ± 0.76 for aDWI, sDWI₁₀₀₀, sDWI₅₀₀ and RSIs respectively. CNR for aDWI and RSIs proved to be significantly different to sDWI ($p < 0.01$) for all patients and patients with csPCa.

Figure 5 compares sDWI, aDWI and RSIs for detection of significant cancer lesions outside of the prostate. For detection of csPCa, the AUCs for sDWI and aDWI were similar in both the prostate and prostate plus 5 mm (Fig. 4 and Table 4). Classification accuracy decreased significantly for sDWI when considering the whole FOV (AUC=0.45 [0.36, 0.54] for sDWI₁₀₀₀ and 0.47 [0.38, 0.56] for sDWI₅₀₀). RSIs was superior to sDWI and aDWI for all ROIs ($p < 0.01$). The AUC of RSIs was 0.77 [0.69, 0.84] within prostate plus 5 mm and decreased to 0.70 [0.61, 0.78] for the whole FOV. FPR90 was similar for aDWI and sDWI in all ROIs. Mean FPR90 was significantly lower for RSIs than for either aDWI or sDWI, indicating fewer false positives ($p < 0.05$).

Discussion

We found that synthesized DWI images can be qualitatively similar to acquired DWI within the prostate even though sDWI is quantitatively an inaccurate representation of aDWI. Moreover, sDWI introduces unacceptable artifacts and inaccuracies in surrounding pelvic tissues. sDWI₅₀₀ calculated using only b -values up to 500 s/mm² was inferior to sDWI₁₀₀₀, demonstrating that the accuracy of sDWI is improved by including higher b -values. Acquiring additional b -values ≤ 1000 s/mm² would further increase the accuracy of the mono-exponential fit and the calculation of sDWI, up to the theoretical limits imposed by a mono-exponential signal model. Beyond b -values of ~ 1000 s/mm², kurtosis effects stemming from the multi-compartmental nature of tissue start to become apparent in the diffusion signal decay, which cannot be accurately modeled using a simple mono-exponential function [33]. Specifically, non-gaussian diffusion of restricted intracellular water results in more signal at high b -values than would be expected for purely gaussian diffusion [34], and therefore a systematic underestimation of high b -value signal by sDWI (Fig. 1). In this study, we showed that the median signal within the prostate was 55–72% lower on sDWI than aDWI. Ideally, b -values greater than 1000 s/mm² should be acquired to ensure that such non-gaussian effects are appropriately measured, enabling the assessment of restricted diffusion and derived biomarkers like RSIs. There is evidence that measurements of restricted intracellular diffusion can help to differentiate between tumors of different histological patterns, like cribriform and non-cribriform, which

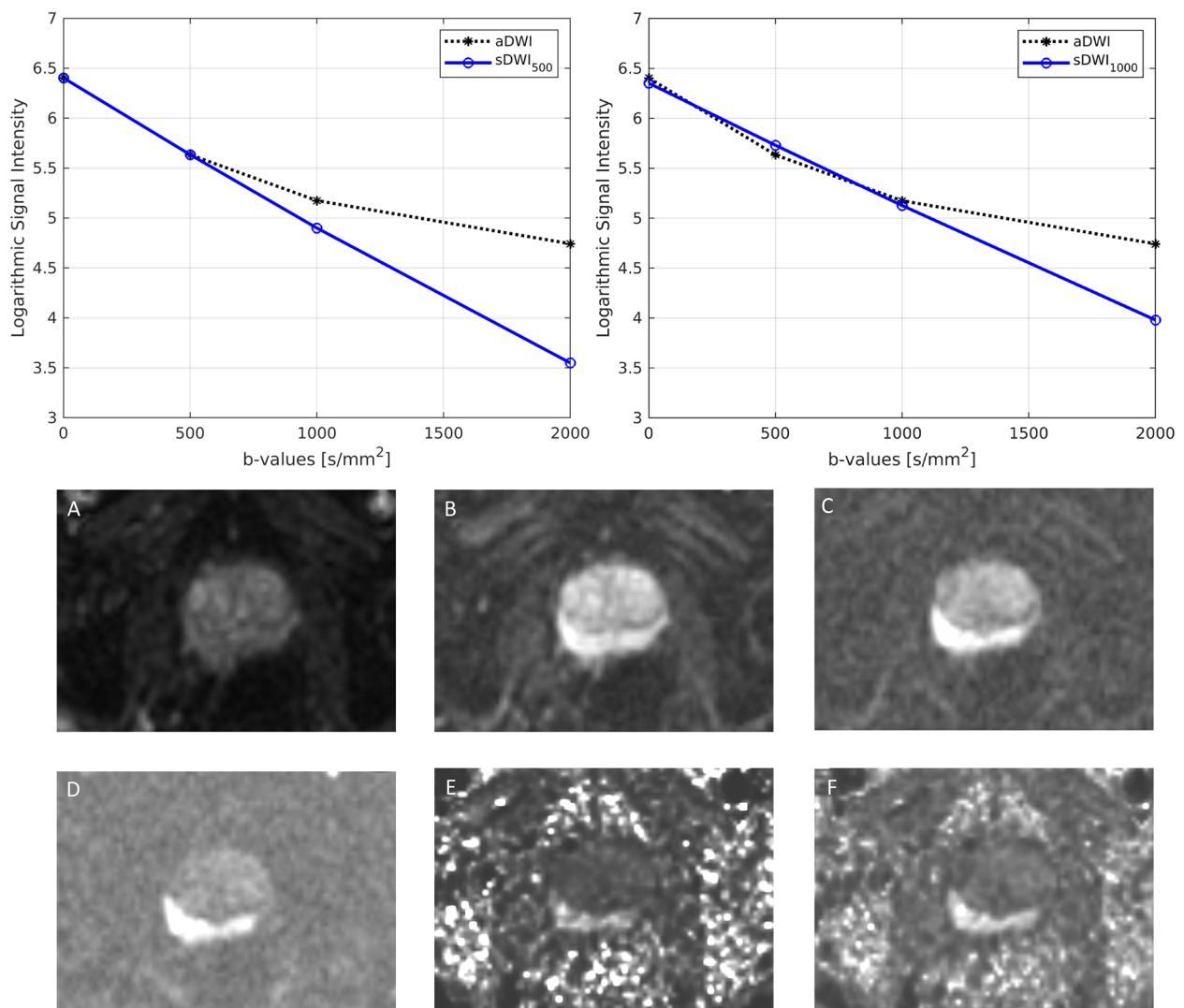


Fig. 1 Comparison of acquired images to those synthesized with mono-exponential models are presented for one representative patient. Mean values within the prostate using either b -values up to 500 s/mm^2 (sDWI_{500}) or b -values up to 1000 (sDWI_{1000}) are compared. Fig. **A–F** show the different diffusion images for one patient. **A–D** presents the acquired images for $b=0 \text{ s/mm}^2$ (**A**), $b=500 \text{ s/mm}^2$ (**B**), $b=1000 \text{ s/mm}^2$ (**C**) and $b=2000 \text{ s/mm}^2$ (**D**). **E** and **F** show the synthesized $b=2000 \text{ s/mm}^2$ images. **E** shows sDWI_{500} and **F** sDWI_{1000} . **aDWI**=acquired diffusion-weighted image for $b=2000 \text{ s/mm}^2$.

differ in the degree of intracellular vs extracellular water [35–37]. The clinical benefits of such granular assessment may offset the increase in scan time necessary to acquire data at higher b -values. Indeed, this study demonstrated a clear improvement in the detection of biopsy-proven csPCa with RSIRs compared to sDWI or aDWI.

Within the prostate and the prostate plus 5 mm margin, lesion conspicuity was reasonably preserved with sDWI. Both sDWI and aDWI had a similar quantitative performance in detecting csPCa with an AUC ranging between 0.56–0.65. However, sDWI introduced larger errors in the surrounding pelvic tissue even in a reduced

FOV acquisition. Because the mono-exponential fitting was performed using a linear fit to log-transformed data for computational efficiency, areas with low SNR were susceptible to significant fitting errors. The pelvic region surrounding the prostate has many such regions with low SNR, including bone and connective tissue with inherently low SNR at the relatively long TEs used in this study, as well as fatty tissue with suppressed signal from the water-selective excitation pulse used during image acquisition.

Severe artifacts were observed on sDWI in these low-SNR regions of the pelvis surrounding the prostate, in

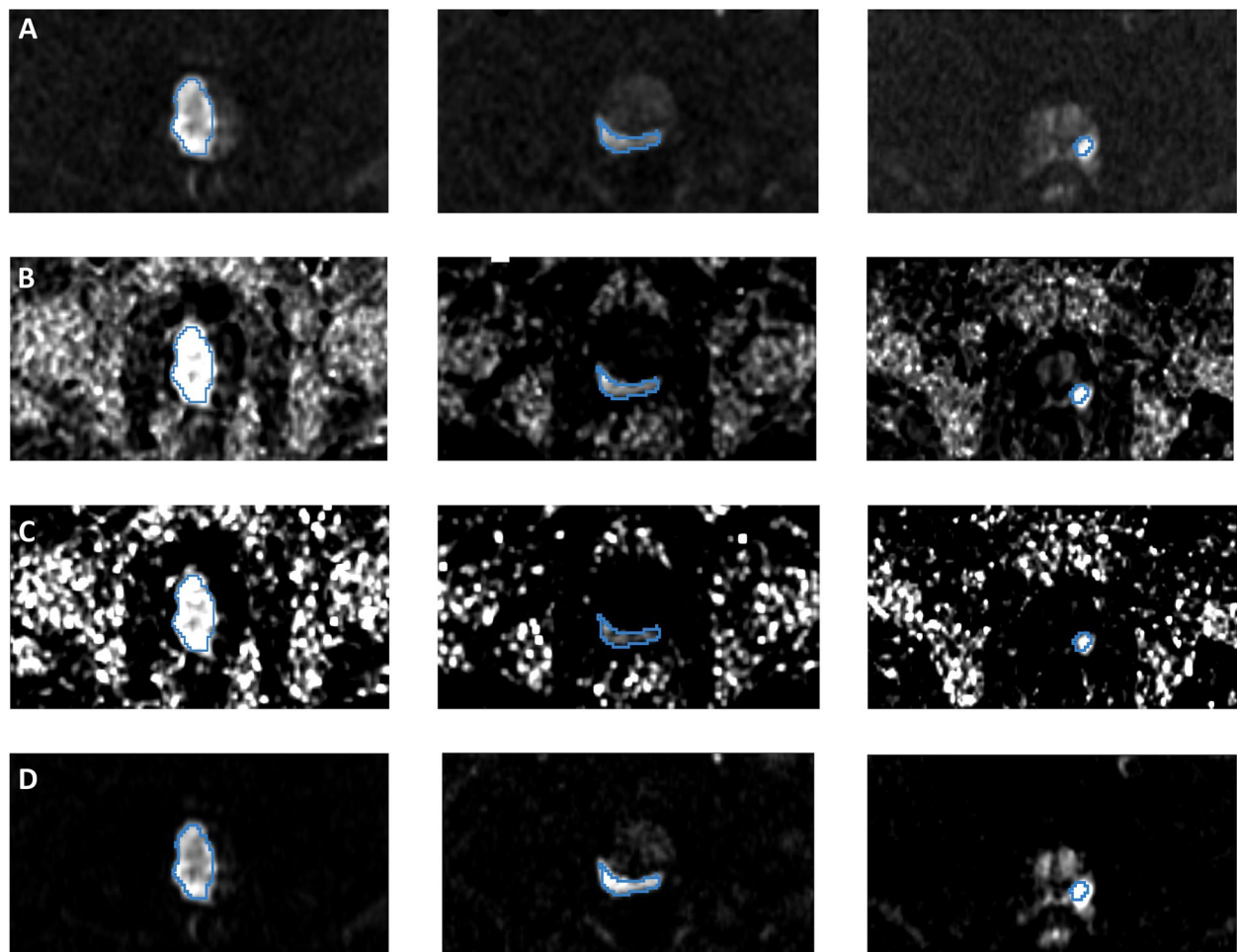


Fig. 2 Representative images from three patients (corresponding to three columns). **A** Acquired diffusion-weighted image (aDWI) for $b=2000\text{s/mm}^2$, **(B)** synthesized DWI using acquired b -values up to $b=1000\text{ s/mm}^2$ (sDWI₁₀₀₀), **(C)** synthesized DWI using acquired values up to $b=500\text{ s/mm}^2$ (sDWI₅₀₀), and **(D)** restriction spectrum imaging restriction score (RSIs). The radiologist-defined cancer lesion for each patient is indicated in blue. All presented patients had a PI-RADS score of 5. The same window level was chosen for all presented images

particular for sDWI₅₀₀, which makes the detection of metastasis outside of the prostate region difficult (Fig. 5). There are many ways to potentially improve the calculation of synthesized images including bi-exponential or multi-exponential modeling [23]. For example, RSIs is based on a multi-exponential model and may synthesize images without introducing artifacts. Image artifacts may be explained by poor signal quality, magnitude smaller than one in a subset of voxels, or noise/distortion correction post image acquisition leading to voxels with extremely low signal intensity. In particular, mono-exponential models fail to correctly represent voxels with low signal intensity due to exponential fitting. Smoother images could be created by censoring those voxels by interpolating from surrounding voxels, smoothing low b -value images prior to calculation, or by thresholding low intensity voxels. For quantitative imaging, the details

of such decisions would need to be clearly described and accounted for, and potentially could lead to more false positive/negative detections. Such enhanced images would not represent the measured truth and would include some unreliable voxels, which must be taken into consideration when interpreting the images. A “nicer looking” image does not necessarily mean that the image quality or reliability is better.

Prior studies reported sDWI to have higher subjective quality and tumor conspicuity [5, 27]. This may reflect the particular imaging sequences and, platforms used, or the particular image enhancement effects. It is also important to note that these prior results were mostly subjective judgements and not quantitative assessments of imaging quality. In the presented study we have proven that tumor conspicuity is quantitatively greater with aDWI (CNR=0.95) in comparison to sDWI

Table 3 Summary of median differences ((sDWI-aDWI)/aDWI) between synthesized (sDWI) and acquired (aDWI) diffusion-weighted imaging. Comparison between sDWI and aDWI is presented relative to aDWI. FOV Field of view

ROI	Datasets	Median Difference ± Interquartile range		
		Total (N = 151)	csPCA (N = 86)	Benign (N = 65)
Lesion	sDWI ₁₀₀₀ vs. aDWI	-47 ± 36%	-43 ± 41%	-48 ± 28%
	sDWI ₅₀₀ vs. aDWI	-63 ± 27%	-60 ± 31%	-67 ± 26%
Prostate	sDWI ₁₀₀₀ vs. aDWI	-55 ± 27%	-52 ± 29%	-59 ± 22%
	sDWI ₅₀₀ vs. aDWI	-72 ± 15%	-69 ± 18%	-74 ± 13%
Prostate + 5 mm margin	sDWI ₁₀₀₀ vs. aDWI	-55 ± 26%	-53 ± 29%	-58 ± 21%
	sDWI ₅₀₀ vs. aDWI	-72 ± 18%	-69 ± 19%	-74 ± 13%
Prostate + 30 mm margin	sDWI ₁₀₀₀ vs. aDWI	-48 ± 35%	-46 ± 41%	-50 ± 28%
	sDWI ₅₀₀ vs. aDWI	-58 ± 34%	-54 ± 45%	-61 ± 23%
Prostate + 70 mm margin	sDWI ₁₀₀₀ vs. aDWI	1.9e19 ± 4.1e19%	1.8e19 ± 3.8e19%	2.0e19 ± 6.4e19%
	sDWI ₅₀₀ vs. aDWI	1.5e47 ± 1.7e48%	1.4e47 ± 1.2e48%	1.5e47 ± 3.0e48%
Whole FOV	sDWI ₁₀₀₀ vs. aDWI	1.1e19 ± 2.3e19%	1.1e19 ± 2.2e19%	1.6e19 ± 2.5e19%
	sDWI ₅₀₀ vs. aDWI	3.4e48 ± 8.9e50%	2.0e48 ± 7.1e50%	1.3e49 ± 9.2e50%

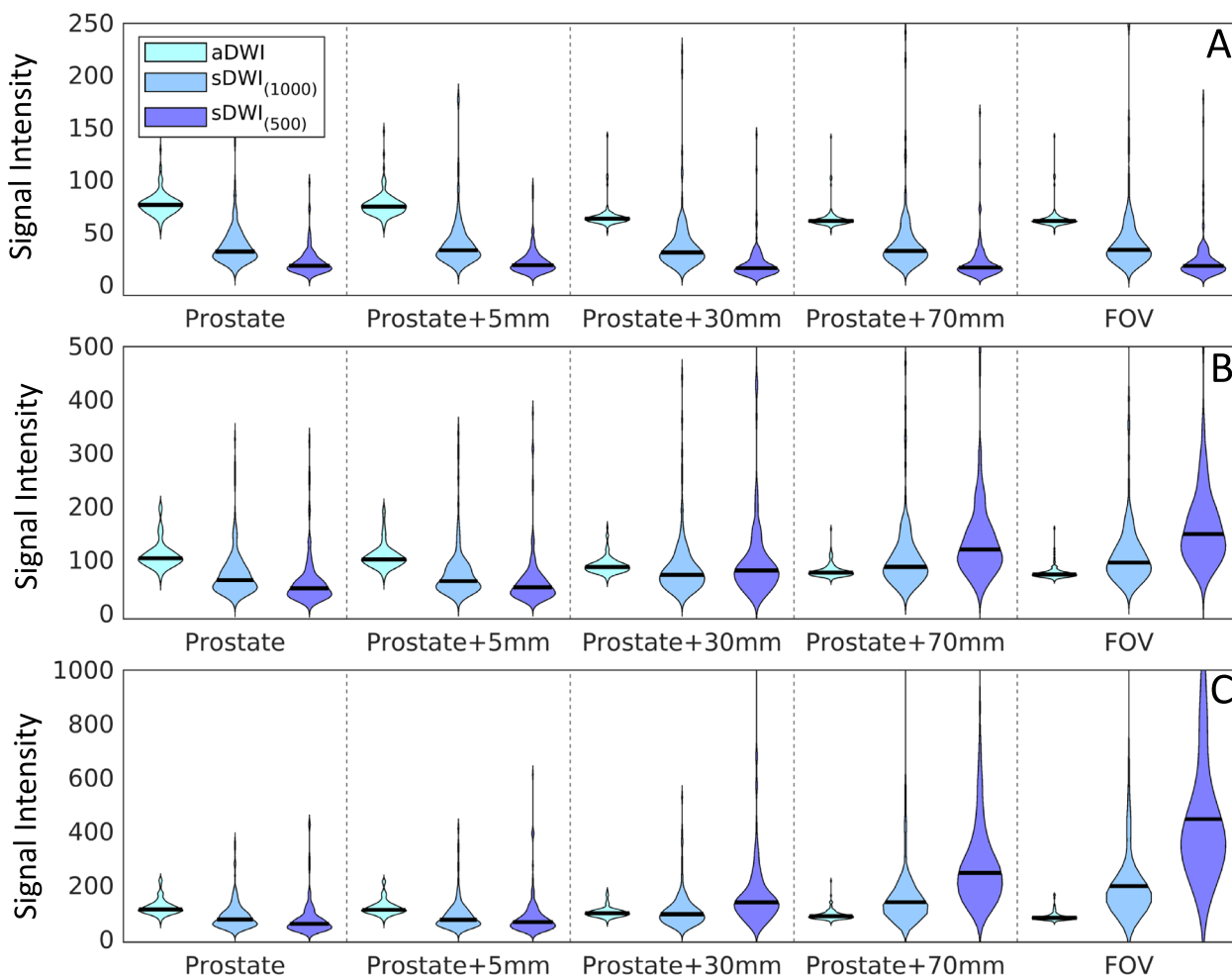


Fig. 3 Violin plots summarizing the signal intensity across 151 patients for (A) 50th percentile, (B) 95th percentile, (C) and 98th percentiles of various DWI metrics calculated for each patient. The percentiles are estimated over different regions of interest: the prostate; the prostate with varying margin (5 mm, 30 mm, or 70 mm); and the whole field of view. aDWI=acquired diffusion-weighted image with $b = 2000\text{s/mm}^2$; sDWI= synthesized DWI for $b = 2000\text{s/mm}^2$ using either acquired b -values up to 1000s/mm^2 (sDWI₁₀₀₀) or up to 500s/mm^2 (sDWI₅₀₀)

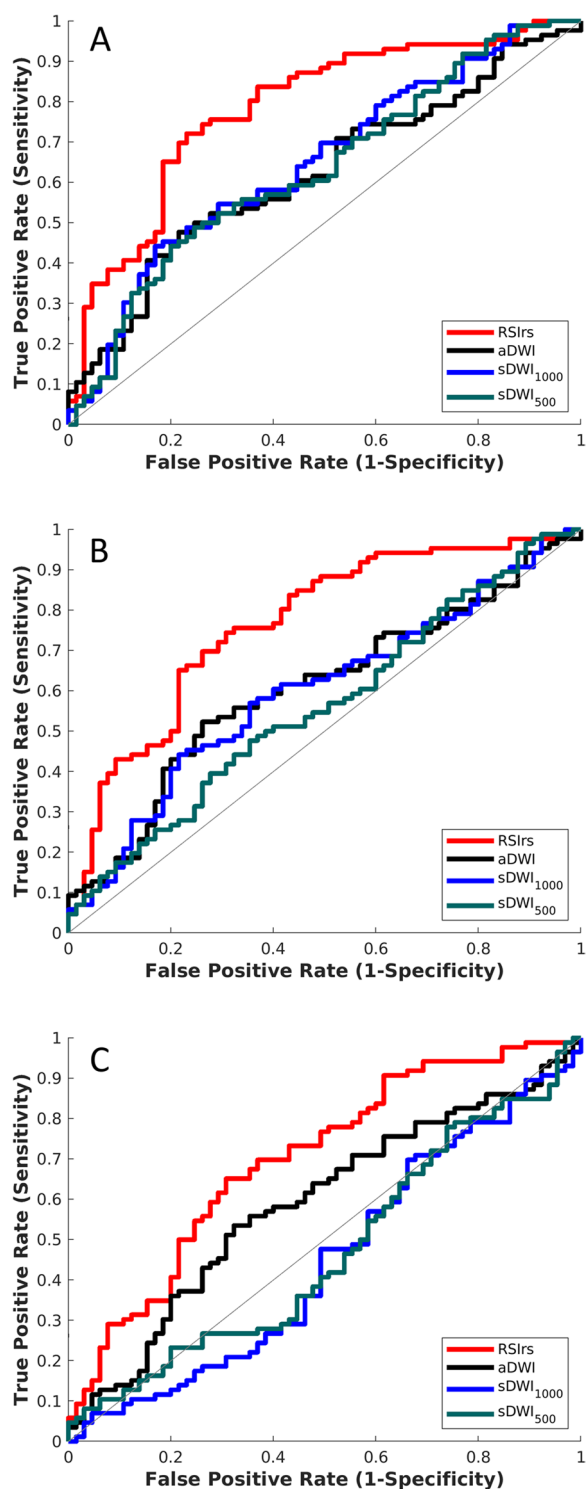


Fig. 4 ROC curves for DWI metrics within three ROIs (A) the prostate, (B) the prostate with 5 mm margin, and (C) the whole field of view. The DWI metrics compared for classification accuracy are RSIRs, acquired diffusion-weighted images (aDWI), synthesized DWI using b -values up to 1000 s/mm^2 (sDWI₁₀₀₀), and synthesized DWI using b -values up to 500 s/mm^2 (sDWI₅₀₀). Clinically significant prostate cancer was defined as a Gleason score ≥ 2

Table 4 Classification accuracy for the detection of cancer is shown for the prostate, prostate plus a 5, 30 and 70 mm margin and the whole field of view (FOV). For statistical comparison bootstrapping ($N = 10,000$) was performed and the 95% confidence intervals (CI) of AUC and the mean false positive rate at 90% sensitivity (FPR90) reported. ROI Region of interest, AUC Area under the curve, RSIRs Biomarker based on restriction spectrum imaging, aDWI Acquired diffusion $b = 2000s/mm^2$ MRI, sDWI₁₀₀₀ Synthesized image using acquired b -values up to 1000 s/mm^2 , sDWI₅₀₀ Synthesized image using acquired b -values up to 500 s/mm^2 , *significantly different with $p < 0.05$ in comparison to each of the other metrics

ROI	Dataset	AUC	95 th CI	FPR90
Prostate	RSIRs	0.78*	0.71–0.86	0.50*
	aDWI	0.62	0.53–0.71	0.82
	sDWI ₁₀₀₀	0.65	0.56–0.73	0.76
	sDWI ₅₀₀	0.63	0.54–0.72	0.76
Prostate + 5 mm margin	RSIRs	0.77*	0.68–0.84	0.53*
	aDWI	0.61	0.51–0.69	0.87
	sDWI ₁₀₀₀	0.60	0.51–0.69	0.84
	sDWI ₅₀₀	0.56	0.47–0.65	0.84
Prostate + 30 mm margin	RSIRs	0.72*	0.64–0.80	0.62*
	aDWI	0.58	0.49–0.67	0.89
	sDWI ₁₀₀₀	0.52	0.43–0.61	0.83
	sDWI ₅₀₀	0.51	0.42–0.61	0.86
Prostate + 70 mm margin	RSIRs	0.72*	0.64–0.81	0.61*
	aDWI	0.60	0.50–0.69	0.88
	sDWI ₁₀₀₀	0.46	0.36–0.55	0.87
	sDWI ₅₀₀	0.45	0.36–0.55	0.89
Whole FOV	RSIRs	0.70*	0.61–0.78	0.62*
	aDWI	0.59*	0.49–0.68	0.90
	sDWI ₁₀₀₀	0.45	0.36–0.54	0.91
	sDWI ₅₀₀	0.47	0.38–0.56	0.90

(CNR = 0.65–0.84). However, an in-depth reader study would be necessary to evaluate the benefits of sDWI over aDWI for contouring, and it might be an interesting topic for future studies. The accuracy in detecting csPCa on a patient-level was assessed by ROC curves. The AUCs proved to be similar for sDWI and aDWI in both the prostate and prostate plus 5 mm. An option to improve the accuracy of DWI is to use a multi-compartment DWI model, e.g., RSIRs, for a more stable and accurate signal extrapolation. For example, RSIRs outperformed both sDWI and aDWI in the present study, see Fig. 4. Other promising multi-compartment models have proved to be superior to conventional multiparametric MRI, like a biomarker derived from VERDICT that outperformed ADC in the detection of csPCa [14]. Hybrid multidimensional MRI acquisitions also showed promising results for classifying csPCa with a reported AUC of 0.94 [33].

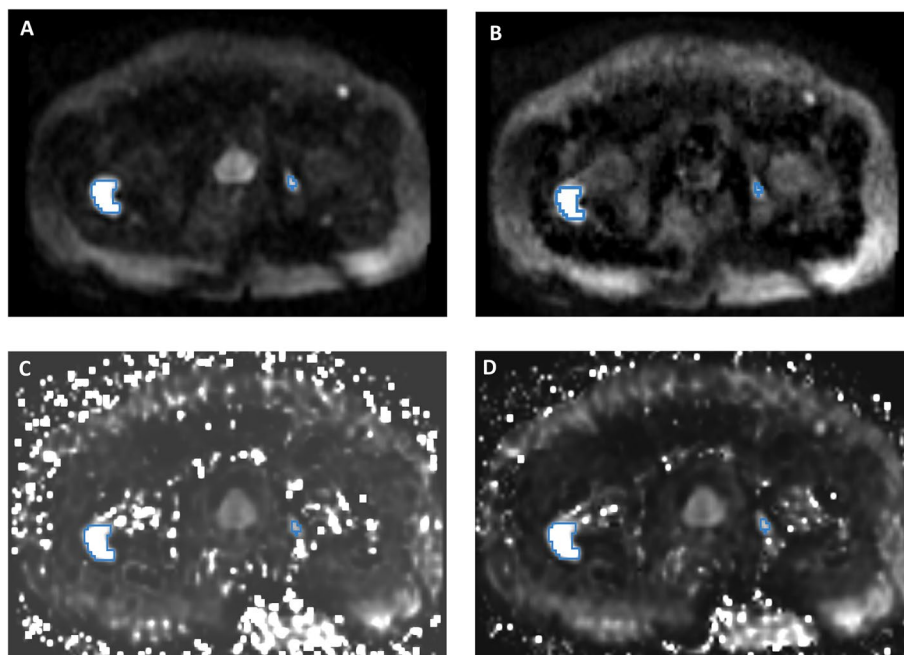


Fig. 5 An example of pelvic DWI in a patient with prostate cancer bone metastases is shown. The blue contours mark the cancer lesions. **A** Acquired DWI with $b=2000$ s/mm²; **(B)** RSIs based on restriction spectrum imaging; **(C)** synthesized DWI using acquired b -values up to 500 s/mm²; and **(D)** synthesized DWI using acquired b -values up to 1000 s/mm². Tumor lesions are easily detectable in **A** and **B**, but there is more high-intensity artifact on sDWI, and the smaller bone metastasis is not as easily identifiable in **C** and **D**

One limiting factor of our study was that we only considered a retrospective dataset from a single scanner and a single institution. Also, the slice thickness of 6 mm for DWI data analyzed here is larger than the 4 mm recommended in PI-RADS v2.1. The larger through-plane voxel size increases signal-to-noise ratio but it is possible some very small tumors could have gone undetected, though any such inaccuracies would apply to aDWI, sDWI, and RSIs alike. Further, only the conventional mono-exponential model was tested in the presented study, as this is the conventional method most cited and used for synthesis of high b -value DWI. A precise comparison of all possible methods for synthesizing DWI is beyond the scope of this manuscript. RSIs is one quantitative biomarker based on a multi-compartment model. The acquisition protocol in the datasets here was not optimized for models like hybrid multi-dimensional MRI or VERDICT.

Conclusions

Within the prostate, sDWI is a systematically inaccurate representation of aDWI, but the techniques are quantitatively comparable in terms of detecting csPCa with an AUC range between 0.56–0.65. In the surrounding pelvic

tissue, high signal intensity artifacts are introduced with sDWI. These artifacts decrease CNR and thus affect the csPCa detection sensitivity in surrounding tissues and might mask potential metastases within the pelvis. RSIs is superior to either sDWI or aDWI for quantitative csPCa detection. Despite the quantitative inaccuracies, sDWI may still be adequate for current subject clinical interpretation within the prostate.

Abbreviations

DWI	Diffusion-weighted imaging
csPCa	Clinically significant prostate cancer
FOV	Field of view
RSIs	Restriction spectrum imaging restriction score
CNR	Contrast-to-noise ratio
sDWI	Synthesized diffusion-weighted image
aDWI	Acquired diffusion-weighted image
ROI	Region of interest
ROC	Receiver operating characteristic
AUC	Area under the curve
FPR90	False positive rate at 90% sensitivity
SNR	Signal-to-noise ratio

Acknowledgements

Not applicable.

Authors' contributions

Conception and design: KK, AC, GK, AD, TS. Administrative support: CC, AZ, AD, TS. Provision of study materials or patients: KK, AZ, AD, TS. Collection and assembly of data: KK, AZ, TH. Data analysis and interpretation: KK, CC, AD, TS. Manuscript writing: All authors. Final approval of manuscript: All authors.

Funding

This work was supported, in part, by the National Institutes of Health (NIH/NIBIB K08EB026503, NIH UL1TR000100), the American Society for Radiation Oncology, and the Prostate Cancer Foundation.

Availability of data and material

The datasets generated during and/or analyzed during the current study are not publicly available due to required IRB approval but are available from the corresponding author on reasonable request.

Declarations

Ethics approval and consent to participate

This retrospective study was approved by the institutional review board at UC San Diego (IRB 805394). The research was performed in accordance with the Declaration of Helsinki, and all relevant regulations. A waiver of consent was approved by the institutional review board for this study as there was minimal risk of harm to patients.

Consent for publication

Not applicable.

Competing interests

AMD is a Founder of and holds equity in CorTechs Labs, Inc, and serves on its Scientific Advisory Board. He is a member of the Scientific Advisory Board of Human Longevity, Inc, and receives funding through research agreements with General Electric Healthcare. RRP is a consultant for Human Longevity, Inc. She also receives funding through research grants from GE Healthcare and Imagine Scientific to UC San Diego; she has an equity interest in CorTechs Labs, Inc, and serves on its Scientific Advisory Board. She also has equity interest in CureMatrix. TMS reports honoraria from Multimodal Imaging Services Corporation, Varian Medical Systems, and WebMD; he has an equity interest in CorTechs Labs, Inc, and serves on its Scientific Advisory Board. These companies might potentially benefit from the research results. The terms of the above arrangements have been reviewed and approved by the University of California San Diego in accordance with its conflict-of-interest policies. Drs. Chatterjee and Karczmar report equity in QMIS LLC, outside the submitted work.

Author details

¹Department of Radiology, University of California San Diego Health, La Jolla, San Diego, CA, USA. ²Department of Radiation Medicine and Applied Sciences, University of California San Diego Health, La Jolla, CA, USA. ³Department of Neurosciences, University of California San Diego Health, La Jolla, San Diego, CA, USA. ⁴Hacıoğlu Data Science Institute, University of California San Diego, La Jolla, San Diego, CA, USA. ⁵Department of Bioengineering, University of California San Diego Jacobs School of Engineering, La Jolla, San Diego, CA, USA. ⁶Department of Radiology, University of Chicago, Chicago, IL, USA. ⁷Sanford J. Grossmann Center of Excellence in Prostate Imaging and Image Guided Therapy, University of Chicago, Chicago, IL, USA.

Received: 19 December 2023 Accepted: 10 June 2024

Published online: 08 July 2024

References

- Turkbey B, Rosenkrantz AB, Haider MA, et al. Prostate Imaging Reporting and Data System Version 2.1: 2019 Update of Prostate Imaging Reporting and Data System Version 2. *Eur Urol*. 2019;2019(76):340–51.
- Tang L, Zhou XJ. Diffusion MRI of Cancer: from Low to High b-Values. *J Magn Reson Imaging JMRI*. 2019;49:23–40.
- Park MJ, Kim YK, Choi S, et al. Preoperative detection of small pancreatic carcinoma: value of adding diffusion-weighted imaging to conventional MR imaging for improving confidence level. *Radiology*. 2014;273:433–43.
- Weinreb JC, Barents JO, Choyke PL, et al. PI-RADS Prostate Imaging - Reporting and Data System: 2015, Version 2. *Eur Urol*. 2016;69:16–40.
- Jendoubi S, Wagner M, Montagne S, et al. MRI for prostate cancer: can computed high b-value DWI replace native acquisitions? *Eur Radiol*. 2019;29:5197–204.
- Shinmoto H, Oshio K, Tanimoto A, et al. Biexponential apparent diffusion coefficients in prostate cancer. *Magn Reson Imaging*. 2009;27:355–9.
- Karunamuni RA, Kuperman J, Seibert TM, et al. Relationship between kurtosis and bi-exponential characterization of high b-value diffusion-weighted imaging: application to prostate cancer. *Acta Radiol Stockh Swed*. 1987;2018(59):1523–9.
- Riches SF, Hawtin K, Charles-Edwards EM, et al. Diffusion-weighted imaging of the prostate and rectal wall: comparison of biexponential and monoexponential modelled diffusion and associated perfusion coefficients. *NMR Biomed*. 2009;22:318–25.
- Le Bihan D, Breton E, Lallemand D, et al. aration of diffusion and perfusion in intravoxel incoherent motion MR imaging. *Radiology*. 1988;168:497–505.
- Rosenkrantz AB, Sigmund EE, Johnson G, et al. Prostate Cancer: Feasibility and Preliminary Experience of a Diffusional Kurtosis Model for Detection and Assessment of Aggressiveness of Peripheral Zone Cancer. *Radiology*. 2012;264:126–35.
- Si Y, Liu R-B. Diagnostic performance of monoexponential DWI versus diffusion kurtosis imaging in prostate cancer: a systematic review and meta-analysis. *AJR Am J Roentgenol*. 2018;211:358–68.
- Panagiotaki E, Chan RW, Dikaos N, et al. Microstructural characterization of normal and malignant human prostate tissue with vascular, extracellular, and restricted diffusion for cytometry in tumours magnetic resonance imaging. *Invest Radiol*. 2015;50:218–27.
- Johnston EW, Bonet-Carne E, Ferizi U, et al. VERDICT MRI for Prostate Cancer: Intracellular Volume Fraction versus Apparent Diffusion Coefficient. *Radiology*. 2019;291:391–7.
- Singh S, Rogers H, Kanber B, et al. Avoiding unnecessary biopsy after multiparametric prostate MRI with VERDICT analysis: The INNOVATE study. *Radiology* 2022;305:212536.
- Chatterjee A, Watson G, Myint E, et al. Changes in epithelium, stroma, and lumen space correlate more strongly with gleason pattern and are stronger predictors of prostate ADC changes than cellularity metrics. *Radiology*. 2015;277:751–62.
- Sadinski M, Karczmar G, Peng Y, et al. Pilot Study of the Use of Hybrid Multidimensional T2-Weighted Imaging-DWI for the Diagnosis of Prostate Cancer and Evaluation of Gleason Score. *AJR Am J Roentgenol*. 2016;207:592–8.
- Chatterjee A, Bourne RM, Wang S, et al. Diagnosis of Prostate Cancer with Noninvasive Estimation of Prostate Tissue Composition by Using Hybrid Multidimensional MR Imaging: A Feasibility Study. *Radiology*. 2018;287:864–73.
- Lee GH, Chatterjee A, Karademir I, et al. Comparing radiologist performance in diagnosing clinically significant prostate cancer with multiparametric versus hybrid multidimensional MRI. *Radiology*. 2022;305:211895.
- Brunsing RL, Schenker-Ahmed NM, White NS, et al. Restriction spectrum imaging: an evolving imaging biomarker in prostate MRI. *J Magn Reson Imaging*. 2017;45:323–36.
- Conlin CC, Feng CH, Rodriguez-Soto AE, et al. Improved characterization of diffusion in normal and cancerous prostate tissue through optimization of multicompartmental signal models. *J Magn Reson Imaging*. 2021;53:628–39.
- Feng CH, Conlin CC, Batra K, et al. Voxel-level Classification of Prostate Cancer on Magnetic Resonance Imaging: Improving Accuracy Using Four-Compartment Restriction Spectrum Imaging. *J Magn Reson Imaging*. 2021;54:975–84.
- Zhong AY, Digma LA, Hussain T, et al. Automated patient-level prostate cancer detection with quantitative diffusion magnetic resonance imaging. *Eur Urol Open Sci*. 2023;47:20–8.
- Liu G, Lu Y, Dai Y, et al. Comparison of mono-exponential, bi-exponential, kurtosis, and fractional-order calculus models of diffusion-weighted imaging in characterizing prostate lesions in transition zone. *Abdom Radiol*. 2021;46:2740–50.
- Maas MC, Fütterer JJ, Scheenen TWJ. Quantitative evaluation of computed high B value diffusion-weighted magnetic resonance imaging of the prostate. *Invest Radiol*. 2013;48:779–86.

25. Sahoo P, Rockne RC, Jung A, et al. Synthetic apparent diffusion coefficient for high b-value diffusion-weighted MRI in prostate. *Prostate Cancer*. 2020;2020:5091218.
26. Blackledge MD, Leach MO, Collins DJ, et al. Computed Diffusion-weighted MR Imaging May Improve Tumor Detection. *Radiology*. 2011;261:573–81.
27. Bittencourt LK, Attenberger UI, Lima D, et al. Feasibility study of computed vs measured high b-value (1400 s/mm²) diffusion-weighted MR images of the prostate. *World J Radiol*. 2014;6:374–80.
28. White NS, McDonald C, McDonald CR, et al. Diffusion-weighted imaging in cancer: physical foundations and applications of restriction spectrum imaging. *Cancer Res*. 2014;74:4638–52.
29. Holland D, Kuperman JM, Dale AM. Efficient correction of inhomogeneous static magnetic field-induced distortion in Echo Planar Imaging. *Neuroimage*. 2010;50:175–83.
30. Zhuang J, Hrabec J, Kangarlu A, et al. Correction of eddy-current distortions in diffusion tensor images using the known directions and strengths of diffusion gradients. *J Magn Reson Imaging*. 2006;24:1188–93.
31. Hintze JL, Nelson RD. Violin plots: a box plot-density trace synergism. *Am Stat*. 1998;52:181–4.
32. DelPriore MR, Biswas D, Hippe DS, et al. Breast cancer conspicuity on computed versus acquired high b-Value diffusion-weighted MRI. *Acad Radiol*. 2021;28:1108–17.
33. Jensen JH, Helpert JA, Ramani A, et al. Diffusional kurtosis imaging: the quantification of non-gaussian water diffusion by means of magnetic resonance imaging. *Magn Reson Med*. 2005;53:1432–40.
34. Brancato V, Cavaliere C, Salvatore M, et al. Non-Gaussian models of diffusion weighted imaging for detection and characterization of prostate cancer: a systematic review and meta-analysis. *Sci Rep*. 2019;9:16837.
35. Liss MA, White NS, Parsons JK, et al. MRI-Derived Restriction Spectrum Imaging Cellularity Index is Associated with High Grade Prostate Cancer on Radical Prostatectomy Specimens. *Front Oncol*; 5. Epub ahead of print 2015. <https://doi.org/10.3389/fonc.2015.00030>
36. Yamin G, Schenker-Ahmed NM, Shabaik A, et al. Voxel Level Radiologic-Pathologic Validation of Restriction Spectrum Imaging Cellularity Index with Gleason Grade in Prostate Cancer. *Clin Cancer Res*. 2016;22:2668–74.
37. Chatterjee Aritick. Validation of Prostate Tissue Composition by Using Hybrid Multidimensional MRI: Correlation with Histologic Findings. <https://doi.org/10.1148/radiol.2021204459>.

Publisher's Note

Springer Nature remains neutral with regard to jurisdictional claims in published maps and institutional affiliations.